2D Materials

RECEIVED
24 February 2015

REVISED
21 April 2015

ACCEPTED FOR PUBLICATION
20 May 2015

PUBLISHED
25 June 2015

PAPERS

Electronic structure and transport in graphene/haeckelite hybrids: an *ab initio* study

Zhen Zhu, Zacharias G Fthenakis and David Tománek

Physics and Astronomy Department, Michigan State University, East Lansing, MI 48824, USA

E-mail: tomanek@pa.msu.edu

Keywords: graphene, haeckelite, hybrid structure, charge transport, DFT

Abstract

We combine *ab initio* density functional theory (DFT) structural studies with DFT-based non-equilibrium Green's function calculations to investigate how the presence of non-hexagonal rings affects electronic transport in graphitic structures. We find that infinite monolayers, finite-width nanoribbons, and nanotubes formed of 5–8 haeckelite with only 5- and 8-membered rings are generally more conductive than their graphene-based counterparts. The presence of haeckelite defect lines in the perfect graphitic structure, a model of grain boundaries in CVD-grown graphene, increases the electronic conductivity and renders it highly anisotropic.

1. Introduction

Graphene is a unique two-dimensional (2D) material that combines extraordinarily high electrical and thermal conductivity [1, 2] with mechanical strength, flexibility, and thermal and chemical stability. Interest in this system increased significantly after a successful mechanical exfoliation using Scotch tape was reported [3] that yielded large, defect-free samples. As a scalable alternative to the 'Scotch tape' exfoliation technique, chemical vapor deposition (CVD) is commonly being used now to form graphene monolayers on metal substrates including Cu [4–6]. The quality of CVD-grown films is inferior to those produced by exfoliation, since gas-phase deposition leads to simultaneous growth of graphene flakes that eventually interconnect, forming grain boundaries with a defective, haeckelite-like structure [7–12] consisting of non-hexagonal carbon rings [13]. Pure haeckelite structures and their hybrids with graphene have a significantly lower thermal conductivity than pure graphene [14]. Only a few theoretical studies have investigated electronic transport in selected graphitic carbon nanostructures with non-hexagonal rings, including hybrid graphene-haeckelite structures [15, 16] and haeckelite nanotubes [17–19].

Here we combine *ab initio* density functional theory (DFT) structural studies with DFT-based nonequilibrium Green's function calculations to investigate how the presence of non-hexagonal rings affects electronic transport in graphitic structures. We find that infinite monolayers, finite-width nanoribbons, and nanotubes formed of 5–8 haeckelite with only 5- and 8-membered rings are generally more conductive than their graphene-based counterparts. The presence of haeckelite defect lines in the perfect graphitic structure, a model of grain boundaries in CVD-grown graphene, increases the electronic conductivity and renders it highly anisotropic.

Haeckelites [7–12] consist of periodic 2D arrangements of non-hexagonal rings of sp^2-bonded carbon atoms. Even though these structures have not been synthesized yet on a large scale, similar atomic arrangements have been observed (i) in 5–7 and 5–8 defect lines forming the in-plane interface between adjacent graphene flakes [13, 20], (ii) in a vitreous atomic network formed during electron-beam irradiation of graphene [21], and (iii) in 5–7 ring structures filling graphene nanoholes during the healing process of these defects [22]. Non-hexagonal rings in graphitic carbon, the arrangement of which is intimately linked to the non-equilibrium growth process, are metastable structures. Effectively, though, these structures are rather stable, as they are protected from structural changes associated with bond rotations by a formidable Stone–Wales activation barrier [23] of $\lesssim$6 eV. Most theoretical studies have focused on the equilibrium structure, stability, and growth stability of haeckelites [7–12, 16, 24–28] and found these systems

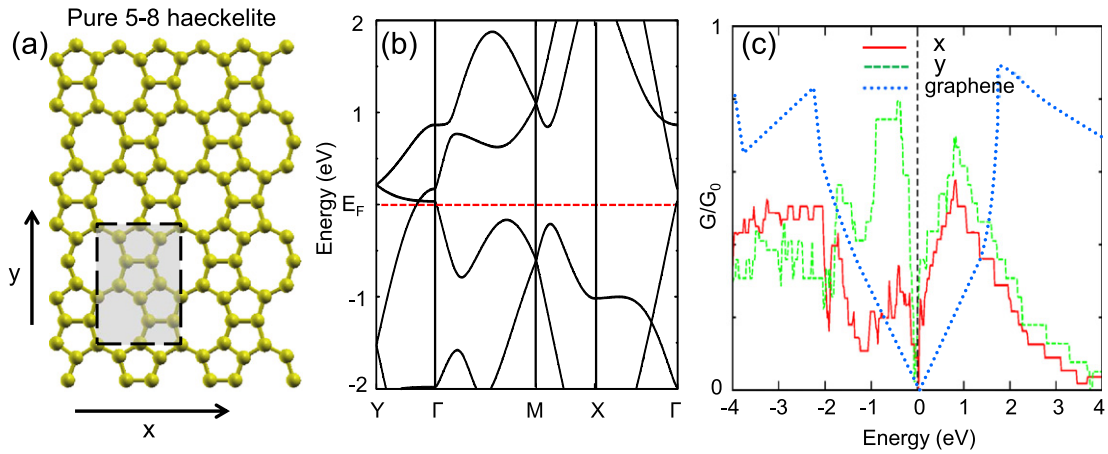

Figure 1. (a) Atomic structure and (b) electronic band structure of 5–8 haeckelite with only 5- and 8-membered rings. The primitive unit cell is indicated by the shaded region. (c) Electronic conductance G/G_0 along the horizontal x-direction, shown by the solid red line, and the vertical y-direction, shown by the dashed green line. G is normalized by the width of the unit cell normal to the transport direction. $E = 0$ corresponds to carrier injection at E_F.

to be either metallic, semi-metallic, or semiconducting [11, 12, 26].

Defects, including lines of non-hexagonal rings or solitons including layer-stacking walls, also occur in few-layer systems, where they affect the local stacking order and effectively decouple the isolated layers near the Fermi level [29–33]. Thus, the interlayer coupling, which is already weak in defect-free graphite, will be further reduced in the presence of defects. Consequently, we expect the electronic properties of defective multi-layer graphene to be represented well by a superposition of isolated monolayers, which are described here.

With continuing interest in CVD-grown graphene as an electronic material, increased attention must be given to carrier scattering at haeckelite-like grain boundaries connecting defect-free graphene regions. The most plausible model geometry to investigate charge transport in polycrystalline graphene is that of interconnected strips of haeckelite and graphene. A consistent picture should be obtained by comparing the effect of different structural arrangements and widths of haeckelite and graphene strips on the conductance and its anisotropy. As a counterpart to transport studies in graphene nanoribbons and nanotubes, we present corresponding results for haeckelite nanoribbons and nanotubes.

2. Methods

To gain insight into the equilibrium structure, stability, and electronic properties of haeckelite structures, we performed DFT calculations as implemented in the SIESTA code [34]. Infinite 2D layers and one-dimensional (1D) ribbons and nanotubes were separated by 10 Å-thick vacuum regions in a three-dimensional (3D) periodic arrangement. We used the Ceperley–Alder [35] exchange-correlation functional as parameterized by Perdew and Zunger [36], norm-conserving Troullier–Martins pseudopotentials [37], and a double-ζ basis, including polarization orbitals. The reciprocal space was sampled by a fine grid [38] of at least $8 \times 8 \times 1$ k-points in the Brillouin zone of the 2D primitive unit cell and its equivalent for 1D structures or larger 2D supercells. We used a mesh cutoff energy of 180 Ry to determine the self-consistent charge density, which provided us with a precision in total energy of $\lesssim 2$ meV/atom. All geometries have been optimized, using the conjugate gradient method [39], until none of the residual Hellmann–Feynman forces exceeded 10^{-2} eV Å^{-1}.

Electronic transport properties were investigated using the nonequilibrium Green function approach, as implemented in the TRAN-SIESTA code [40]. Ballistic transport calculations for optimized structures were performed using a single-ζ basis with polarization orbitals, a 180 Ry mesh cutoff energy, and the same k-point grid [38] as used for structure optimization.

3. Results and discussion

3.1. 5-8 haeckelite

A perfect 2D monolayer of 5–8 haeckelite containing only 5- and 8-membered rings is shown in figure 1(a). The optimum rectangular unit cell is spanned by the Bravais lattice vectors $a_1 = 4.87$ Å in the x-direction and $a_2 = 6.93$ Å in the y-direction. The 5–8 haeckelite structure is about 0.36 eV/atom less stable than graphene, which is comparable to the stability of narrow carbon nanotubes. Due to this relatively high stability, we expect 5–8 haeckelite structures to coexits with graphene at grain boundaries.

The electronic band structure of 5–8 haeckelite is presented in figure 1(b). In contrast to semimetallic graphene, 5–8 haeckelite is metallic and has a finite

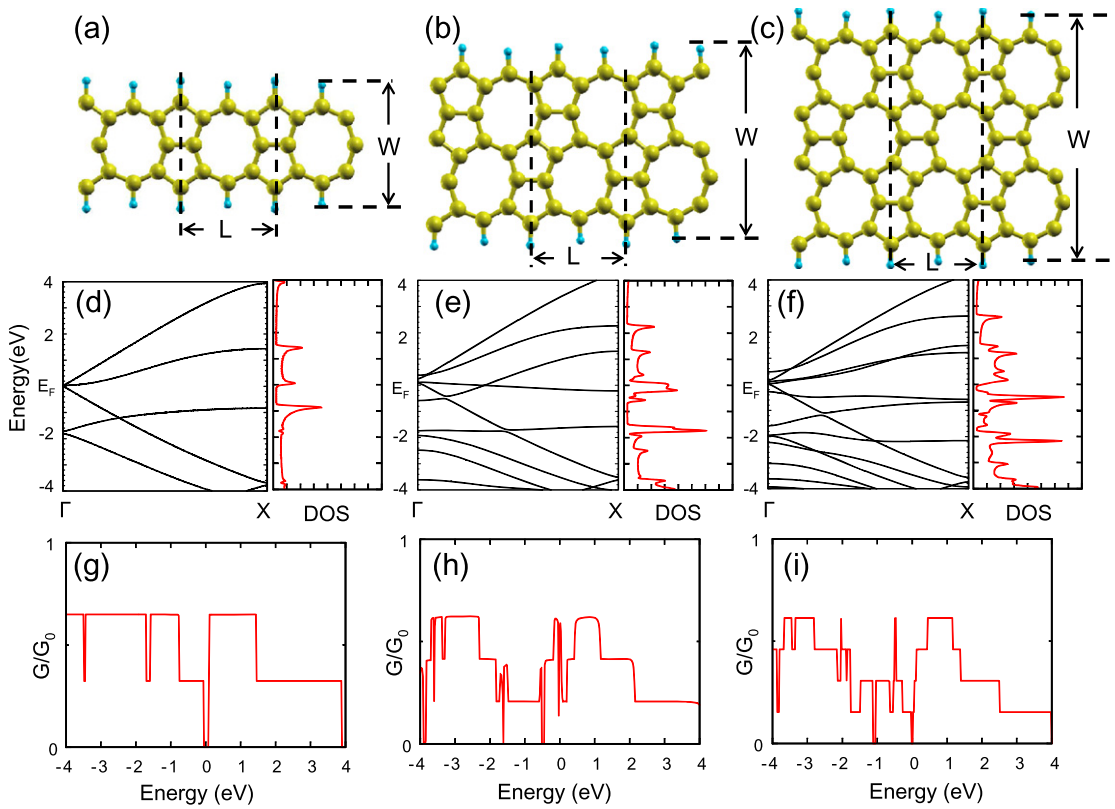

Figure 2. Atomic structure, electronic band structure, and transport properties of haeckelite nanoribbons passivated by hydrogen at the edge. The atomic structure of haeckelite nanoribbons with various width is shown in (a), (b), and (c). The corresponding electronic band structure and density of states is shown in (d), (e), and (f), and ballistic transport conductance G/G_0 in (g), (h), and (i). The density of state is given per atom.

electronic density of states at the Fermi level. Whereas the Fermi surface of graphene consists of six isolated k-points, that of 5–8 haeckelite is a line of finite length that intersects the Γ–Y high-symmetry line, as seen in figure 1(b). This anisotropy in the electronic band structure clearly reflects the anisotropy in the arrangement of carbon rings in the lattice structure, which can be viewed as chains of pentagons that are interconnected.

There is no clear one-to-one correspondence between quantum transport and the electronic band structure. Whereas electronic band structure along specific directions in k-space and the density of states are useful to distinguish a metal from a semiconductor, this information is not completely sufficient to predict quantum conductance behavior. Even though the presence of a fundamental bandgap in a semiconductor suppresses any conduction, particular metallic systems with a nonzero density of states at the Fermi level may still display a transport gap if a particular conduction channel is blocked.

The results of our quantum transport calculation for the 5–8 haeckelite are shown in figure 1(c). Besides the improved conductivity over graphene, suggested by the increased density of states at the Fermi level, we find the conductivity to be also anisotropic, as expected when considering the atomic arrangement in figure 1(a). We find the electrical conductance along the y-direction to be much higher than along the x-direction and even observe a very narrow transport gap at E_F. These findings are consistent with a very anisotropic Fermi surface that crosses the Γ–Y, but not the Γ–X, high-symmetry line in figure 1(b).

3.2. 5-8 haeckelite nanoribbons and nanotubes

Finite-width graphene nanoribbons and carbon nanotubes have received wide attention, since—unlike infinite graphene monolayers—some of these structures display sizeable band gaps. In analogy to these structures, we also studied quantum transport in 1D haeckelite nanoribbons (h-NRs) and nanotubes (h-NTs). In figure 2, we present our results for h-NRs with different widths W that are passivated by hydrogen at the edge. The atomic structure of the three narrowest haeckelite nanoribbons is shown in figures 2(a)–(c). We find the optimum lattice constant $L \approx 4.9$ Å to be nearly independent of the width W. We also note that structures in figures 2(a) and (c) have mirror symmetry, whereas that in figure 2(b) does not.

As seen in panels (d)–(i) of figure 2, we found the electronic structure and conductance of h-NRs to depend sensitively on the ribbon width. Structures

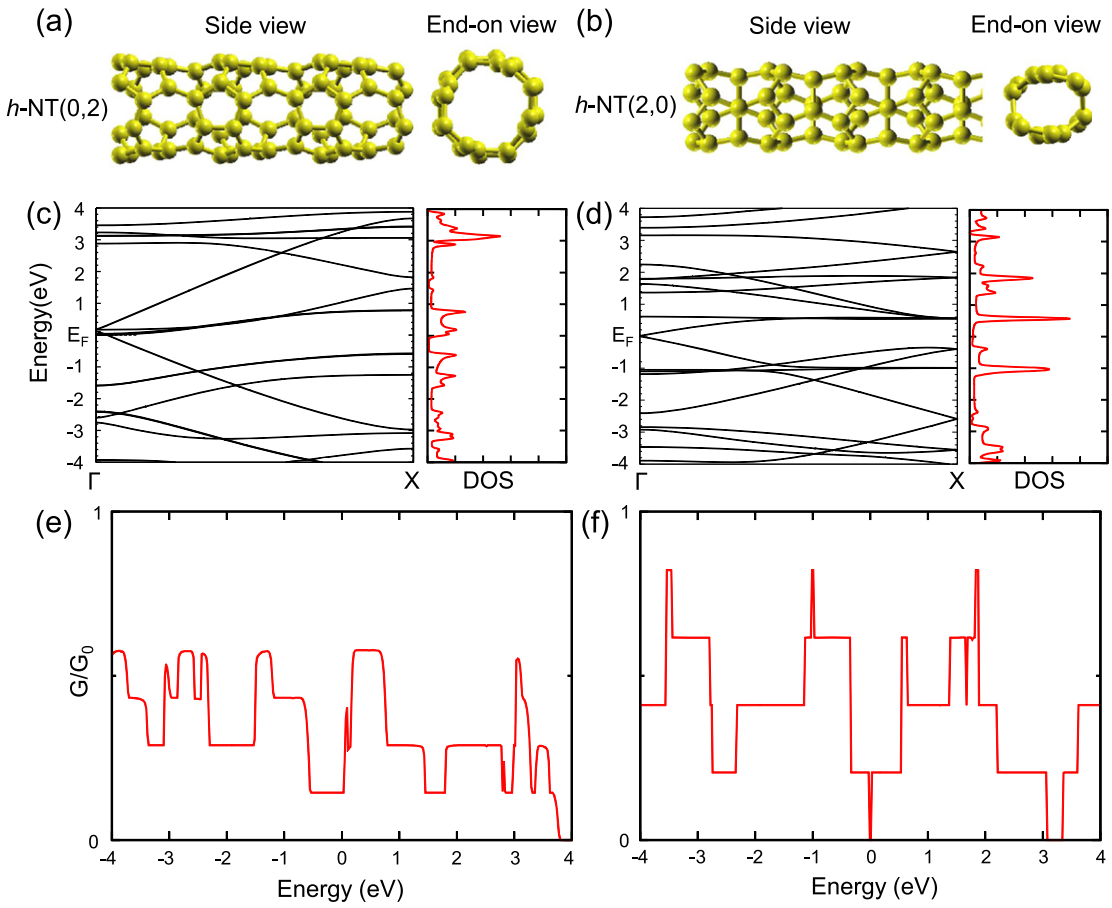

Figure 3. Structural and electronic properties of haeckelite nanotubes. Atomic structure of (a) h-NT(0, 2) and (b) h-NT(2, 0) nanotubes. The length of the unit cells is denoted by L and the width by W. The corresponding electronic band structure and density of states is shown in (c) and (d), and ballistic transport conductance G/G_0 in (e) and (f). The density of state is given per atom.

with an odd number of 8-membered rings in the unit cell, depicted in figures 2(a) and (c), are narrow-gap semiconductors, with the fundamental bandgap decreasing with increasing width, from $E_g = 0.05$ eV in figures 2(a) and (d) to $E_g = 0.02$ eV in figures 2(c) and (f). Structures with an even number of 8-membered rings in the unit cell are all metallic. One example with two 8-membered rings in the unit cell is shown in figures 2(b) and (e). Quantum conductance G of the three h-NRs in units of the conductance quantum G_0 is shown in figures 2(g)–(i). Of most interest is the presence or absence of a transport gap at $E = 0$, corresponding to carrier injection at E_F. As expected, the semiconducting nanoribbons depicted in figures 2(a) and (c) also have a finite transport gap, seen in figures 2(g) and (i). The metallic nanoribbon in figure 2(b) does not have a transport gap at $E = 0$, according to figure 2(h).

Similar to graphene-based carbon nanotubes, we can construct 5–8 haeckelite-based nanotubes and characterize them by the chiral index (n, m) in analogy to carbon nanotubes. We present the structure and electronic properties of two representative 5–8 haeckelite nanotubes, h-NT(0, 2) and h-NT(2, 0), in figure 3. Both the side and the end-on view of these nanotubes in figures 3(a) and (b) indicate that their optimum cross section is not as round and their surface not as smooth as that of their graphitic counterparts, owing to the presence of 5- and 8-membered rings. We found the ultra-narrow h-NT(0, 2) and h-NT(2, 0) nanotubes to be stable but highly strained. The stability of the narrower h-NT(2, 0) is lower by 0.81 eV/atom and that of the wider h-NT(0, 2) is lower by 0.45 eV/atom with respect to the planar haeckelite structure depicted in figure 1(a).

The electronic band structure and density of states of the h-NT(0, 2) nanotube, shown in figure 3(c), indicate that h-NT(0, 2) is metallic and has a non-zero density of state at the Fermi energy. As expected, also the calculated quantum conductance, shown in figure 3(e), indicates non-vanishing quantum conductance at $E = 0$. Quite different are the electronic structure and quantum conductance results for the h-NT(2, 0) nanotube, shown in figures 3(d) and (f), which display a very small fundamental and transport gap of <0.1 eV. Unlike in graphene-based carbon nanotubes, there is no general rule to predict whether a given h-NT nanotube should be metallic or semiconducting.

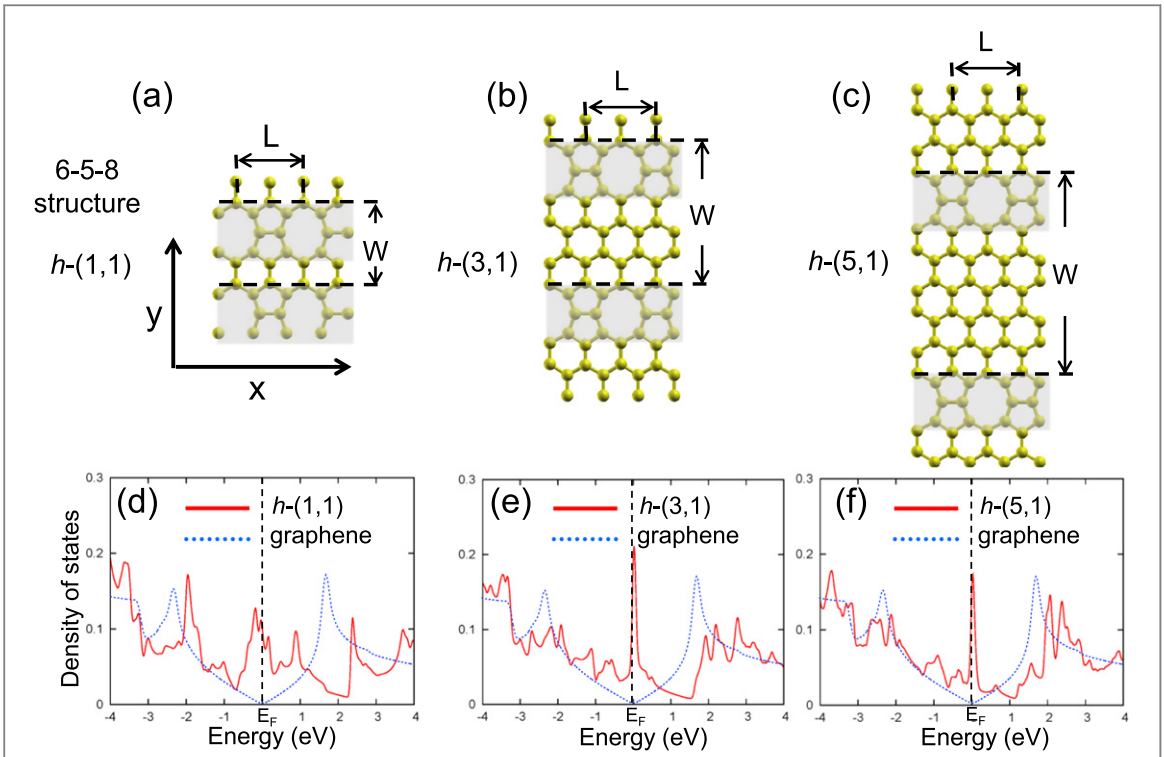

Figure 4. Structure and electronic properties of hybrid haeckelite/graphene structures h-(n,m) consisting of graphene strips interconnected by 5–8 haeckelite strips, with n referring to the width of graphene and m to that of haeckelite. The upper panels depict the atomic structure of (a) h-(1, 1), (b) h-(3, 1), and (c) h-(5, 1) hybrid structures with $m = 1$. The corresponding electronic densities of states are shown in the lower panels (d), (e), and (f). The length of the unit cells is denoted by L and the width by W. The density of state is given per atom.

3.3. Hybrid haeckelite-graphene structures

As a model of haeckelite-like grain boundaries connecting graphene grains in polycrystalline graphene samples, we construct hybrid haeckelite-graphene structures consisting of strips of 5–8 h-NRs of various widths interconnecting bare zigzag graphene nanoribbons with different widths. The hybrid systems, identified as h-(n, m), are characterized by the number m of eight-membered rings per unit cell and the number n of hexagonal rings across the width of the unit cell. We explored two families of hybrid structures with $m = 1$ and $m = 2$ but different values of n. These studies let us explore how the density of 5–8 line defects should affect the electronic and transport properties of the hybrid structures.

The optimum atomic arrangement and electronic structure of h-(n, 1) hybrids, with $n = 1, 3, 5$, is shown in figure 4. We found all the structures to be metallic, as indicated by the peak in electronic densities of states at the Fermi energy in figures 4(d)–(f). Since the density of states in defect-free graphene, shown by the dotted line in figures 4(d)–(f), vanishes at E_F, any new states at the Fermi level must be associated with structural defects, such as 5–8 defects in our case. We have verified this by inspecting the charge distribution associated with the peak at E_F in defective graphene. We may also expect that the relative importance of these states will decrease with increasing dilution of defects. To better quantify the relative importance of defect states, we defined a new quantity

$$\langle \Delta N\,(\Delta E)\rangle = \int_{E_F-\Delta E}^{E_F+\Delta E} \left[N_{\rm def}\left(E\right) - N_{\rm gra}\left(E\right)\right]^2 {\rm d}E, \qquad (1)$$

where $N_{\rm def}(E)$ is the electronic density of state of defective graphene, $N_{\rm gra}$ is the corresponding quantity in pristine graphene (normalized per atom), and ΔE defines an energy window around E_F. Clearly, $\langle \Delta N\,(\Delta E)\rangle$ will decrease with decreasing fraction of defects. We have confirmed this trend and indeed see a decrease in the value of $\langle \Delta N\,(\Delta E)\rangle$ in h-(n, 1) hybrids, with increasing n, as the pristine graphene strips become wider.

The corresponding results for h-(n, 2) hybrids with wider haeckelite strips ($m = 2$) and also wider graphene strips characterized by $n = 2, 4, 6$ are shown in figure 5. Similar to the $m = 1$ family presented in figure 4, also the h-(n, 2) structures are all metallic, but the peak in the density of states peak near E_F does not appear as sharp as in the h-(n, 1) structures. Similar to h-(n, 1) hybrids, the effect of the defect line diminished with increasing n.

For the sake of illustration, we included the density of states of pristine graphene in the same energy range and observe that the presence of 5–8 haeckelite line defects increases the density of states near the Fermi level, benefitting conductivity.

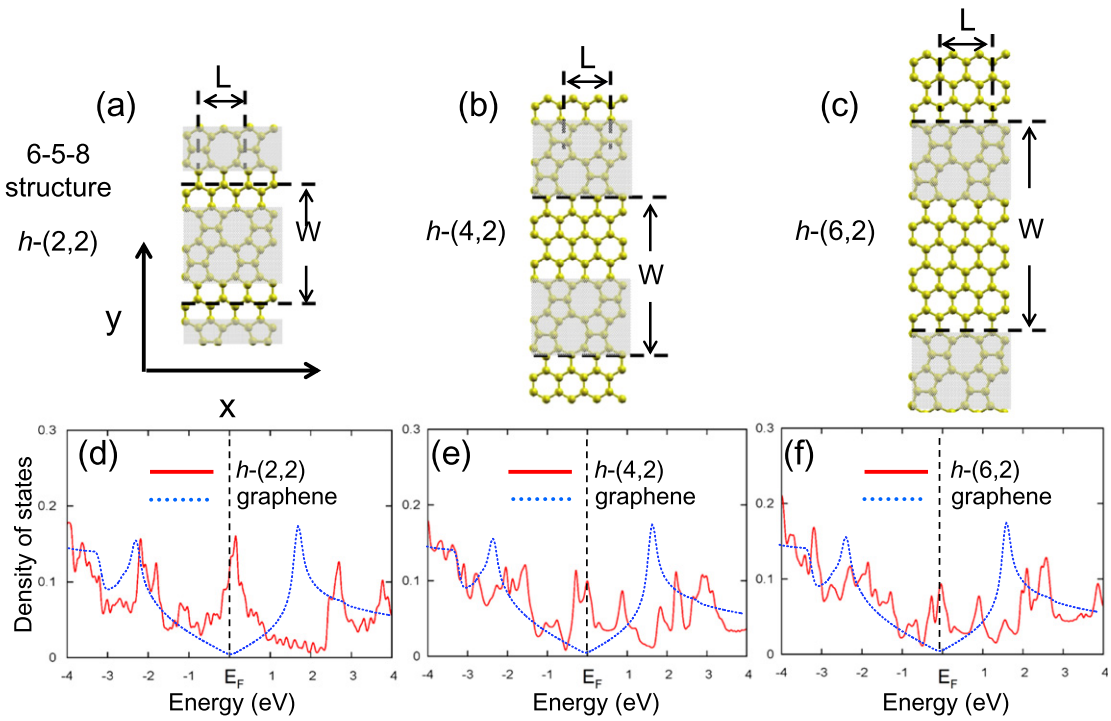

Figure 5. Structure and electronic properties of hybrid haeckelite/graphene structures h-(n,m), consisting of graphene strips interconnected by 5–8 haeckelite strips, with n referring to the width of graphene and m to that of haeckelite. The upper panels depict the atomic structure of (a) h-(2, 2), (b) h-(4, 2), and (c) h-(6, 2) hybrid structures with $m = 2$. The corresponding electronic densities of state are shown in the lower panels (d), (e), and (f). The length of the unit cells is denoted by L and the width by W. The density of state is given per atom.

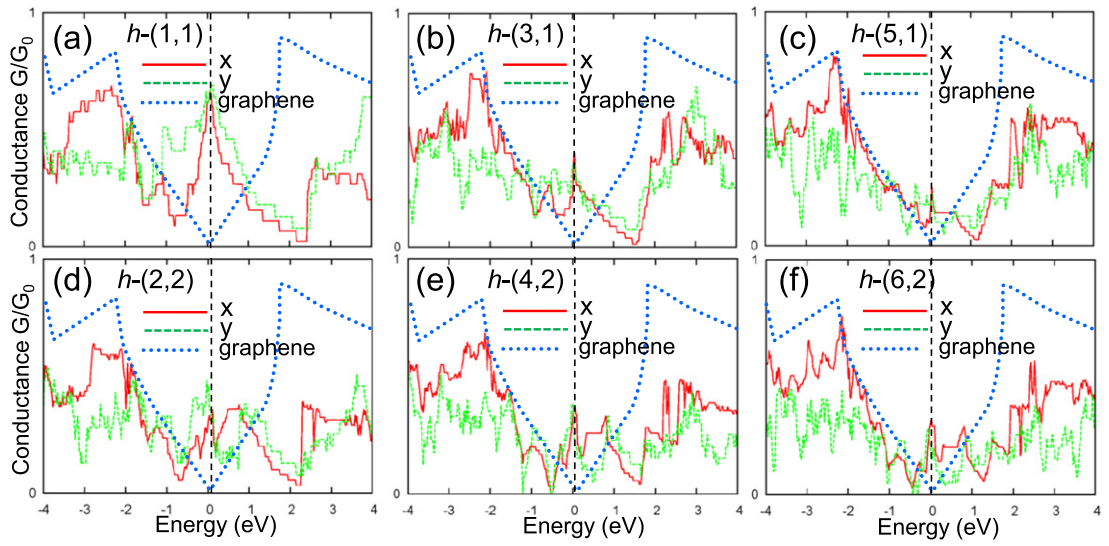

Figure 6. Electronic conductance G of hybrid haeckelite/graphene structures h-(n,m), consisting of graphene strips interconnected by 5–8 haeckelite strips. Results are presented for (a) h-(1, 1), (b) h-(3, 1), (c) h-(5, 1), (d) h-(2, 2), (e) h-(4, 2), and (f) h-(6, 2) with different widths n of the graphene strips and m of the haeckelite strips. The structures and transport directions are defined in Figures 4(a)–(c) and 5(a)–(c). G is normalized by the width of the unit cell normal to the transport direction. $E = 0$ corresponds to carrier injection at E_F.

We note that the narrow haeckelite strips within the h-(n, 1) hybrid structures correspond to the free-standing, but hydrogen-passivated, nanoribbon presented in figure 2(a). Similarly, also the wider haeckelite strips within the h-(n, 2) hybrid structures have a counterpart in the free-standing, but hydrogen-passivated, nanoribbon presented in figure 2(b). Comparison between the density of states of the free-standing haeckelite nanoribbons in figures 2(d) and (e) and the densities of states in figures 4(d)–(f) and figures 5(d)–(f) indicates that the electronic structure of free-standing and embedded nanoribbons is very different.

The increasing similarity of h-(n, m) structures with increasing width n of the graphene strips and defect-free graphene is also reflected in the quantum conductance of these systems, shown in figure 6. Unlike the density of states, quantum conductance is anisotropic. Especially for large values of n, transport along the defect lines will increasingly resemble that of graphene superposed with that of the conducting defect lines acting as quantum conductors or metal wires. We conclude that lines of non-hexagonal rings at grain boundaries in polycrystalline graphene should enhance the conductance of this system over pristine semimetallic graphene.

4. Conclusions

In conclusion, we have combined *ab initio* DFT structural studies with DFT-based nonequilibrium Green's function calculations to study how the presence of non-hexagonal rings affects electronic transport in graphitic structures found in polycrystalline graphene. We found that infinite monolayers, finite-width nanoribbons, and nanotubes formed of 5–8 haeckelite with only 5- and 8-membered rings are generally more conductive than their graphene-based counterparts. The presence of haeckelite defect lines in the perfect graphitic structure, a model of grain boundaries in CVD-grown graphene, increases the electronic conductivity and renders it highly anisotropic.

Acknowledgments

The authors acknowledge financial support from the National Science Foundation Cooperative Agreement No. EEC-0832785, titled 'NSEC: Center for High-rate Nanomanufacturing'. Computational resources have been provided by the Michigan State University High Performance Computing Center.

References

[1] Novoselov K S, Geim A K, Morozov S V, Jiang D, Zhang Y, Dubonos S V, Grigorieva I V and Firsov A A 2004 *Science* **306** 666–9
[2] Bolotin K, Sikes K, Jiang Z, Klima M, Fudenberg G, Hone J, Kim P and Stormer H 2008 *Solid State Commun.* **146** 351–5
[3] Novoselov K S, Jiang D, Schedin F, Booth T J, Khotkevich V V, Morozov S V and Geim A K 2005 *Proc. Natl Acad. Sci. USA* **102** 10451–3
[4] Kim K S, Zhao Y, Jang H, Lee S Y, Kim J M, Kim K S, Ahn J H, Kim P, Choi J Y and Hong B H 2009 *Nature* **457** 706–10
[5] Reina A, Jia X, Ho J, Nezich D, Son H, Bulovic V, Dresselhaus M S and Kong J 2009 *Nano Lett.* **9** 30–35
[6] Li X *et al* 2009 *Science* **324** 1312–4
[7] Crespi V H, Benedict L X, Cohen M L and Louie S G 1996 *Phys. Rev.* B **53** R13303–5
[8] Terrones H, Terrones M, Hernández E, Grobert N, Charlier J C and Ajayan P M 2000 *Phys. Rev. Lett.* **84** 1716–9
[9] Wang X Q, Li H D and Wang J T 2013 *Phys. Chem. Chem. Phys.* **15** 2024–30
[10] Lusk M T and Carr L D 2008 *Phys. Rev. Lett.* **100** 175503
[11] Appelhans D J, Lin Z and Lusk M T 2010 *Phys. Rev.* B **82** 073410
[12] Appelhans D J, Carr L D and Lusk M T 2010 *New J. Phys.* **12** 125006
[13] Huang P Y *et al* 2011 *Nature* **469** 389–92
[14] Fthenakis Z G, Zhu Z and Tománek D 2014 *Phys. Rev.* B **89** 125421
[15] Botello-Méndez A R, Cruz-Silva E, López-Urías F, Sumpter B G, Meunier V, Terrones M and Terrones H 2009 *ACS Nano* **3** 3606–12
[16] Rocquefelte X, Rignanese G M, Meunier V, Terrones H, Terrones M and Charlier J C 2004 *Nano Lett.* **4** 805–10
[17] Lisenkov S, Andriotis A N, Ponomareva I and Menon M 2005 *Phys. Rev.* B **72** 113401
[18] Li Y F, Li B R and Zhang H L 2008 *J. Phys.: Cond. Matter* **20** 415207
[19] Popović Z, Milošević I and Damnjanović M 2011 *Mater. Sci. Eng.* B **176** 494–6
[20] Lahiri J, Lin Y, Bozkurt P, Oleynik I I and Batzill M 2010 *Nat. Nanotechnol.* **5** 326–9
[21] Eder F R, Kotakoski J, Kaiser U and Meyer J C 2014 *Sci. Rep.* **4** 4060
[22] Zan R, Ramasse Q M, Bangert U and Novoselov K S 2012 *Nano Lett.* **12** 3936–40
[23] Tománek D 2014 *Guide Through the Nanocarbon Jungle* (Bristol: IOP Publishing) doi:10.1088/978-1-627-05273-3
[24] Wang Y, Page A J, Nishimoto Y, Qian H J, Morokuma K and Irle S 2011 *J. Am. Chem. Soc.* **133** 18837–42
[25] Enyashin A N and Ivanovskii A L 2011 *Phys. Status Solidi (b)* **248** 1879–83
[26] Su C, Jiang H and Feng J 2013 *Phys. Rev.* B **87** 075453
[27] Sheng X L, Cui H J, Ye F, Yan Q B, Zheng Q R and Su G 2012 *J. Appl. Phys.* **112** 074315
[28] Liu Y, Wang G, Huang Q, Guo L and Chen X 2012 *Phys. Rev. Lett.* **108** 225505
[29] Zhang F, MacDonald A H and Mele E J 2013 *Proc. Natl Acad. Sci.* **110** 10546–51
[30] Alden J S, Tsen A W, Huang P Y, Hovden R, Brown L, Park J, Muller D A and McEuen P L 2013 *Proc. Natl Acad. Sci.* **110** 11256–60
[31] Brown L, Hovden R, Huang P, Wojcik M, Muller D A and Park J 2012 *Nano Lett.* **12** 1609–15
[32] San-Jose P, Gorbachev R V, Geim A K, Novoselov K S and Guinea F 2014 *Nano Lett.* **14** 2052–7
[33] Nagapriya K S, Berber S, Cohen-Karni T, Segev L, Srur-Lavi O, Tomanek D and Joselevich E 2008 *Phys. Rev. B* **78** 165417
[34] Artacho E *et al* 2008 *J. Phys.: Cond. Matter* **20** 064208
[35] Ceperley D M and Alder B J 1980 *Phys. Rev. Lett.* **45** 566–9
[36] Perdew J P and Zunger A 1981 *Phys. Rev.* B **23** 5048–79
[37] Troullier N and Martins J L 1991 *Phys. Rev.* B **43** 1993–2006
[38] Monkhorst H J and Pack J D 1976 *Phys. Rev.* B **13** 5188–92
[39] Hestenes M R and Stiefel E 1952 *J. Res. Natl Bur. Stand.* **49** 409–36
[40] Brandbyge M, Mozos J L, Ordejón P, Taylor J and Stokbro K 2002 *Phys. Rev.* B **65** 165401